Glycobiology vol. 21 no. 7 pp. 934–948, 2011
doi:10.1093/glycob/cwr026
Advance Access publication on March 18, 2011

Secondary cell wall polysaccharides from *Bacillus cereus* strains G9241, 03BB87 and 03BB102 causing fatal pneumonia share similar glycosyl structures with the polysaccharides from *Bacillus anthracis*

L Scott Forsberg[2], Biswa Choudhury[3], Christine Leoff[2], Chung K Marston[4], Alex R Hoffmaster[4], Elke Saile[4], Conrad P Quinn[4], Elmar L Kannenberg[2], and Russell W Carlson[1,2]

[2]Complex Carbohydrate Research Center, University of Georgia, 315 Riverbend Road, Athens, GA 30602, USA; [3]Glycotechnology Core Resource, University of California at San Diego, San Diego, CA, USA; [4]Centers for Disease Control and Prevention, 1600 Clifton Road, Atlanta, GA 30333, USA

Received on January 31, 2011; revised on March 3, 2011; accepted on March 4, 2011

Secondary cell wall polysaccharides (SCWPs) are important structural components of the *Bacillus* cell wall and contribute to the array of antigens presented by these organisms in both spore and vegetative forms. We previously found that antisera raised to *Bacillus anthracis* spore preparations cross-reacted with SCWPs isolated from several strains of pathogenic *B. cereus*, but did not react with other phylogenetically related but nonpathogenic *Bacilli*, suggesting that the SCWP from *B. anthracis* and pathogenic *B. cereus* strains share specific structural features. In this study, SCWPs from three strains of *B. cereus* causing severe or fatal pneumonia (G9241, 03BB87 and 03BB102) were isolated and subjected to structural analysis and their structures were compared to SCWPs from *B. anthracis*. Complete structural analysis was performed for the *B. cereus* G9241 SCWP using NMR spectroscopy, mass spectrometry and derivatization methods. The analyses show that SCWPs from *B. cereus* G9241 has a glycosyl backbone identical to that of *B. anthracis* SCWP, consisting of multiple trisaccharide repeats of: →6)-α-D-Glc*p*NAc-(1 → 4)-β-D-Man*p*NAc-(1 → 4)-β-D-Glc*p*NAc-(1→. Both the *B. anthracis* and pathogenic *B. cereus* SCWPs are highly substituted at all GlcNAc residues with α- and β-Gal residues, however, only the SCWPs from *B. cereus* G9241 and 03BB87 carry an additional α-Gal substitution at O-3 of ManNAc residues, a feature lacking in the *B. anthracis* SCWPs. Both the *B. anthracis* and *B. cereus* SCWPs are pyruvylated, with an approximate molecular mass of 12,000 Da. The implications of these findings regarding pathogenicity and cell wall structure are discussed.

Keywords: Bacillus anthracis / *Bacillus cereus* / cell wall / polysaccharide / structure

Introduction

Members of the group *Bacillus cereus* are Gram-positive, spore-forming bacilli that include the closely related species *B. anthracis*, *B. cereus* and *B. thuringiensis*. These organisms reside mainly in soil and on vegetation, where contact with *B. anthracis* may lead to anthrax, predominantly in livestock and less commonly in humans. *B. cereus* is primarily associated with food poisoning, characterized by bacilli that produce emetic or diarrhoeal toxins (CDC 1990, 1996; Hoffmaster et al. 2008), and it is also an opportunistic pathogen that can cause localized and severe systemic infections, e.g. bacteremia, septicemia, endocarditis, meningitis or pneumonia. There have been several recent reports describing *B. cereus* pneumonias that were atypically severe or fatal in metalworkers (CDC 1996; Miller et al. 1997).

Using multilocus sequence typing (MLST), the phylogenetic characterization of the *B. cereus* strains described in this study (strains G9241, 03BB87 and 03BB102) showed that they were close relatives to *B. anthracis* (Hoffmaster et al. 2004, 2008). Detailed genetic characterization of the isolates revealed that all three strains contained plasmids related to the *B. anthracis* pXO1 virulence plasmid harboring many of the pXO1 genes including the toxin genes *pagA*, *lef* and *cya* that encode for protective antigen, lethal factor and edema factor (Hoffmaster et al. 2006). Two of the strains, *B. cereus* G9241 and 03BB87, additionally carried the circular plasmid pBC218 which is thought to be involved in the production of a polysaccharide capsule (Hoffmaster et al. 2004). The genes *capA*, *capB* and *capC* that are required for the poly-D-γ-glutamic acid capsule synthesis in *B. anthracis* were detected in *B. cereus* 03BB102. However, while capsule production of some type could be demonstrated in all three clinical isolates, none produced the poly-D-γ-glutamic acid

[1]To whom correspondence should be addressed: Tel: +1-706-542-4439; Fax: +1-706-542-4412; e-mail: rcarlson@ccrc.uga.edu

capsule (Hoffmaster et al. 2004, 2006) characteristic of *B. anthracis*.

The secondary cell wall polysaccharides (SCWPs) of bacilli, particularly those producing an external S-protein layer, are structurally distinct from the teichoic acids synthesized by other Gram-positive organisms and appear to serve unique and specific functions for a cell surface polysaccharide. The structures of SCWPs from various nonpathogenic *Bacillus* have been reviewed (Schäffer and Messner 2005) and are typically rich in hexosamine and hexosaminuronic acids, often with linear di- and tetrasaccharide repeating units with minimal branching. Like teichoic acids, these 'nonclassical' SCWPs are linked at the reducing end to peptidoglycan muramic acid residues by labile phosphate esters (Schäffer and Messner 2005). Several studies have demonstrated a central role for these SCWPs as mediators in the anchoring and/or targeting of proteins to the cell surface, including the S-layer proteins, through noncovalent interactions with a conserved domain in these proteins known as surface layer homology (SLH) domain (Mesnage et al. 1999, 2000; Kern et al. 2010). The presence of pyruvate acetal on the polysaccharide mediator may be essential for binding (Mesnage et al. 2000; Schäffer and Messner 2005; Kern et al. 2010). At present, it is not known whether these SCWPs have other essential functions in cell architecture, for example, in capsule formation or in functions important for cell viability and virulence. Furthermore, immunological evidence (Leoff et al. 2009) suggests that these SCWPs are expressed in the spore coat; yet their arrangement and means of attachment within the spore layers are not known.

Recently, we compared the cell wall glycosyl composition of a variety of *B. anthracis* and *B. cereus* strains, including the above-described *B. cereus* clinical isolates and demonstrated that a compositional variation correlates with differences in phylogenetic relatedness (Leoff, Saile et al. 2008). We also isolated the SCWP (previously referred to as HF-PS since the SCWP is released from the cell wall by treatment with aqueous HF) from three strains of *B. anthracis* and the nonpathogenic *B. cereus* strain ATCC10987 and described their structures (Choudhury et al. 2006; Leoff, Choudhury et al. 2008, Leoff, Saile et al. 2008). For the *B. anthracis* strains examined to date, these results indicate that the SCWPs are species-specific cell wall structures having a conserved structural motif of a repeating *N*-acetyl hexosamine trisaccharide backbone in which two of the three aminoglycosyl residues are *N*-acetylmannosamine (ManNAc) and *N*-acetylglucosamine (GlcNAc) and the third is either GalNAc or GlcNAc (Choudhury et al. 2006). In all of these strains, the hexosamine backbone is highly substituted with monosaccharides. Additionally, we observed that SCWPs from *B. anthracis* is immunogenic and that antisera generated from live and killed *B. anthracis* Sterne $34F_2$ spore preparations react specifically with the SCWP from all *B. anthracis* strains tested, but not with the SCWP from *B. cereus*-type strain ATCC 14579 or strain ATCC 10987 (Leoff, Choudhury et al. 2008). However, these *B. anthracis* antisera did show cross-reactivity against the SCWP of the pathogenic *B. cereus* strains G9241, 03BB87 and 03BB102 (Leoff, Choudhury et al. 2008, Leoff et al. 2009), indicating that their structures may be similar to that of *B. anthracis*.

It is intriguing that the SCWPs from *B. anthracis* strains are all identical to one another but differ from the SCWPs from investigated nonpathogenic *B. cereus* strains. On the other hand, the cross-reactivity of the anti-$SCWP_{Ba}$ antiserum with the pathogenic *B. cereus* strains causing human pneumonia (Leoff, Choudhury et al. 2008, Leoff et al. 2009) suggests structural similarities in the SCWP of these strains with that of *B. anthracis*. Moreover, it raises the question as to whether structural similarities in the SCWP in these strains are a precondition for their severe virulence properties. Using indirect fluorescent antibody staining, in this study we address these questions with an extended search for cross-reactivity of anti-$SCWP_{Ba}$ antiserum with a set of *B. cereus* clinical isolates originating from patients with gastrointestinal and other severe diseases (Hoffmaster et al. 2008). In addition, we structurally investigate in detail the SCWP from pathogenic strain *B. cereus* G9241 using nuclear magnetic resonance (NMR), mass spectrometric and gas chromatographic analyses and compare it with the SCWP structure from *B. anthracis* (Choudhury et al. 2006).

Results

Immunofluorescence of Bacillus *strains*

B. cereus G9241 vegetative cells were subjected to immunofluorescence using anti-$SCWP_{Ba}$ antiserum as the primary antibody (Figure 1). The photograph shows intense overall reactivity; however, staining was not homogeneous with some cells reacting less intensely. Within each cell, staining did not appear to be evenly distributed; the strongest staining appeared associated with cell walls and possibly areas undergoing or related to cell division. Clearly, antiserum raised to purified *B. anthracis* SCWPs also reacts strongly with these *B. cereus* cells, indicating that similar glycosyl epitopes exist on these cells.

Cross-reactivity of anti-$SCWP_{Ba}$ antiserum with a range of B. cereus *clinical isolates*

As shown in Table I, among the strains tested under growth conditions described, cross-reactivity of the anti-$SCWP_{Ba}$

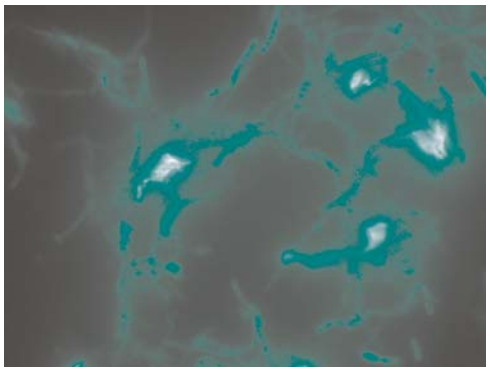

Fig. 1. Immunofluorescence labeling of *B. cereus* G9241 clinical isolates with anti-$SCWP_{Ba}$ antisera. Intense cross-reactivity of the pathogenic *B. cereus* G9241 vegetative cells with antisera raised to the *B. anthracis* SCWP reveals similar cell surface glycosyl epitopes on these strains. The nonpathogenic *B. cereus*-type strain ATCC 14579 yields no staining with the anti-$SCWP_{Ba}$ antisera.

Table I. Reactivity of anti-HFPS$_{B.anthracis}$ antiserum with *B. cereus* clinical isolates

ID	MLST clade[a]	MLST subtype[a]	Clinical information	DFA result
B. anthracis Sterne[b]	1	2	Vaccine strain	+
G9241	1	ST78	P	+
03BB102	1	11	P,f	+
D4214	1	62	S	+
03BB87	1	78	P,f	+
F7720	1	141	G	+
H3076.97	1	144	G,e; F	−
H1548	1	90	Sf	−
B1357	1	91	S	−
F5191	1	122	S	Weak +
H2573.97	1	26	G,e; F,e	−
H9311	1	26	G,e; F,e	−
F666	1	92	G	−
C1783	1	123	G	−
C3276	2	136	S	−
SB460	2	146	S	−
F6722	2	4	F	−
G9844	2	56	G	−
F438	2	98	G	−
G2055	2	99	G	−
3297	2	124	G	−
F3920	2	94	P	−
G4200	2	95	P,f	−
1952	2	101	S,f	−
F4794	2	111	P	−
04S 00334	2	85	S	−
B4266	2	89	P,f	−
ATCC 14579[c]	2	4	F	−

[a]Clades and subtypes on the basis of MLST as described in Hoffmaster et al. (2008).
[b]Strain *B. anthracis* Sterne 34F$_2$ (positive control) and *B. cereus* ATCC 14579 (negative control).
ID refers to the *B. cereus* isolate number. P, pneumonia; f, fatal; S, severe; G, gastrointestinal; e, emetic; F, food-borne; DFA, direct fluorescent antibody staining.

antiserum was restricted to *B. cereus* strains that phylogenetically are restricted to the MLST Clade 1. No cross-reactivity was observed to any of the MLST Clade 2 *B. cereus* strains. Within the MLST Clade 1 including the control strains, 7 from 14 strains (or 50%) reacted positive with the antiserum, including strains *B. cereus* G9241, 03BB87 and 03BB102. From the strains isolated from patients with severe disease symptoms or pneumonia, only two isolates, strains *B. cereus* H1548 and B1357, were negative with the antiserum. All pneumonia-associated isolates in Clade 1 reacted positively with the antiserum, while none of the pneumonia-associated strains within Clade 2 reacted with anti-SCWP$_{Ba}$ antiserum. To compare anti-SCWP$_{Ba}$ antiserum-positive SCWP structures from *B. cereus* with the HF-PS structure from *B. anthracis*, we investigated the SCWPs from strains *B. cereus* G9241, 03BB87 and 03BB102 in some detail.

Fractionation and molecular mass estimation

SCWPs from *B. cereus* G9241, 03BB87, 03BB102, ATCC 14579 and *B. anthracis* Sterne were chromatographed on a Superose-12 size exclusion column (Supplementary data, Figure S1). This procedure was effective in removing other polymeric components and provided a useful estimate of molecular mass (MM) for the SCWP from various *Bacillus* strains. The *B. cereus* G9241 SCWP showed slightly faster chromatographic mobility than the 11,000 Da dextran standard, suggesting an MM of ∼12 kDa. The SCWPs from various *B. anthracis* strains, including Sterne 34F$_2$, appeared to have a similar size profile, while the *B. cereus*-type strain, ATCC 14579, indicated a greater mass of ∼20 kDa, with a more restricted size distribution compared with other SCWPs (Supplementary data, Figure S1). These profiles indicate that the SCWPs released by HF treatment are indeed polysaccharides of notable size and not simply a series of small oligosaccharides as frequently reported. Several strains, particularly those from *B. anthracis*, contained variable amounts of a high MM glucan which eluted at the void volume and may correspond to a glycogen-storage polysaccharide reported previously (Slock and Stahly 1974; Kiel et al. 1994; Takata et al. 1997).

Glycosyl composition and linkage analysis

Composition analysis of the Superose-purified SCWPs from the three *B. cereus* strains isolated from cases of pneumonia (strains G9241, 03BB87 and 03BB102) showed that all were very similar to that of the *B. anthracis* strains, consisting of galactose (Gal), GlcNAc and ManNAc in approximately 3:2:1 ratio. These glycosyl compositions are markedly different from SCWPs from various nonpathogenic *B. cereus* strains, including *Bc*-type strains ATCC 10987 and ATCC 14579 (reviewed in Leoff, Saile et al. 2008). Analysis of the diastereomeric derivatives indicated an absolute D-configuration for all glycosyl components in the *B. cereus* G9241 and *B. anthracis* SCWPs. The Superose-purified SCWP fractions were free of muramic acid and amino acids (e.g. those characteristic of peptidoglycan).

Glycosyl linkage analysis of SCWPs from *B. anthracis* Ames showed terminal Gal, 3,4-linked GlcNAc, 3,4,6-linked GlcNAc and 4-linked ManNAc (Choudhury et al. 2006). The *B. cereus* G9241, 03BB87 and 03BB102 SCWPs showed the presence of these same linkages and, possibly, 3,4-linked ManNAc along with greater heterogeneity in the ratios of other differently linked amino sugars than in the *B. anthracis* SCWP. These results, together with the immunological results, indicated some structural similarity between the *B. anthracis* and pathogenic *B. cereus* SCWPs.

Mass spectrometry analysis of SCWP-derived oligosaccharides

Our initial attempts to isolate the intact SCWPs by release with HF-treatment yielded, in addition to a polymeric fraction, a lower MM fraction which could be isolated by size exclusion chromatography (SEC) on Bio-Gel P-2 column (Choudhury et al. 2006). This lower MM fraction was examined by matrix-assisted laser desorption ionization-time of flight (MALDI-TOF) mass spectrometry and the spectra of the SCWP-derived oligosaccharides from *B. anthracis* Ames and the pathogenic *B. cereus* strains are shown in Figure 2. In all spectra, the molecular ion *m/z* 1136 represents the sodiated MM of a hexasaccharide repeating unit, consistent with $[Hex_3HexNAc_3 + Na]^+$. The molecular ion with mass of 974

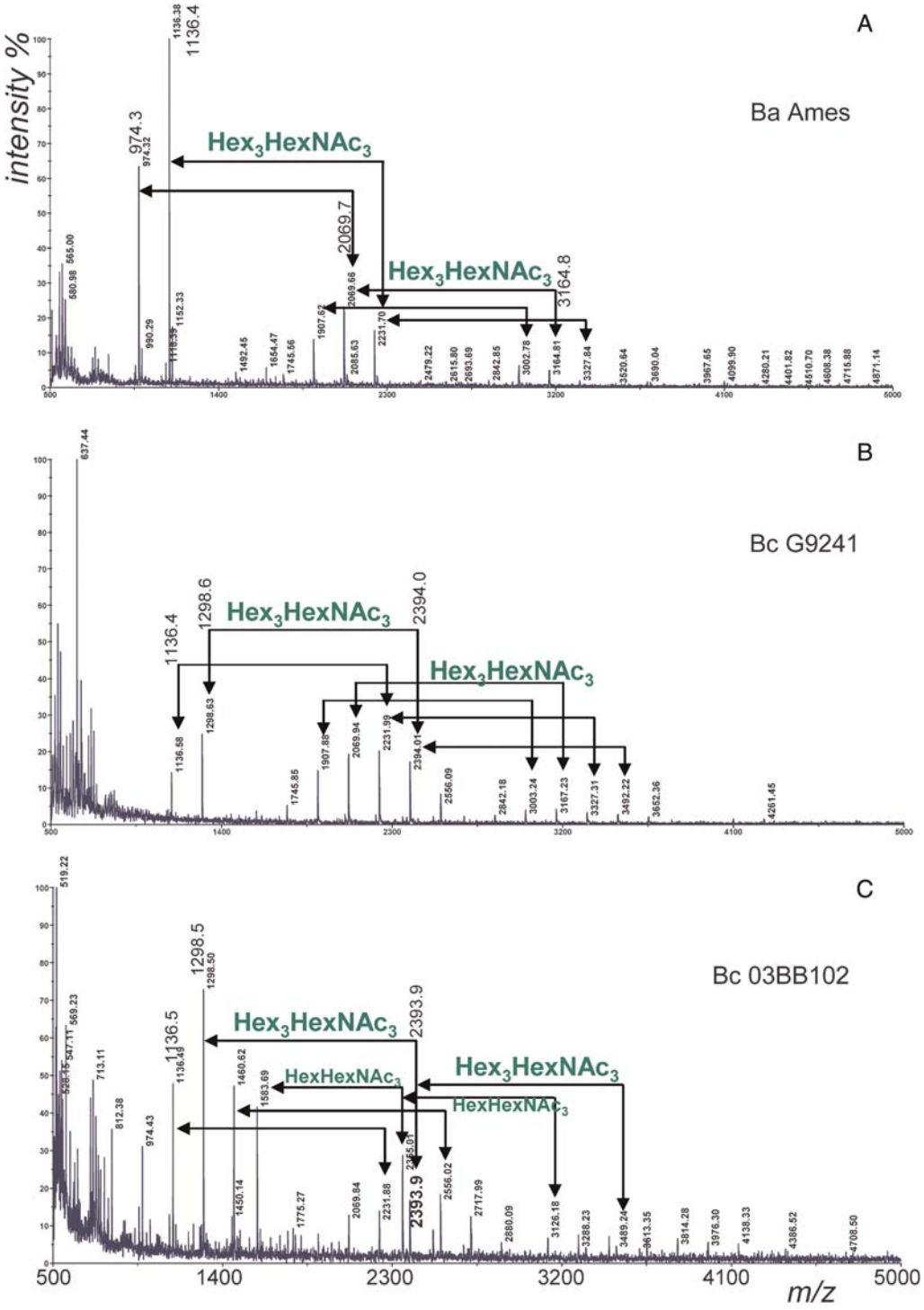

Fig. 2. Positive-ion MALDI-TOF mass spectra of SCWP-derived oligosaccharides (OSs) isolated from different *Bacillus* strains. (**A**) *B. anthracis* Ames; (**B**) *B. cereus* G9241; and (**C**) *B. cereus* 03BB102. The OSs from *B. cereus* strain 03BB87 gives identical results as shown for strain G9241. Ions are sodiated species of the form $[M+Na]^{+1}$. In all spectra, the molecular ion with mass of 1136 represents the sodiated MM of the hexasaccharide repeating unit ($Hex_3HexNAc_3$). The molecular ion with mass of 974 indicates the presence of this repeating unit less one hexose (i.e. Gal). The next cluster of ions with mass 2232 represents the dimer of the hexasaccharide, and ions with *m/z* 2070 and 1908 are, respectively, one and two Gal units less than the dimer. The SCWP from all *B. cereus* and *B. anthracis* strains showed the presence of these same ions, indicating the presence of conserved structural features. However, ions with more, as well as less, Gal substitutions were also observed in the *B. cereus* SCWP compared with *B. anthracis* SCWPs, indicating additional heterogeneity of the secondary cell wall structures in these pathogenic *B. cereus* strains. The *B. cereus* 03BB102 SCWP shows additional complexity, with increments corresponding to ($Hex_1HexNAc_3$), to be described in a separate report.

Table II. Positive-ion MALDI-TOF analysis of oligosaccharides derived from the SCWPs from *B. anthracis* and pathogenic *B. cereus*

Strains	*B. anthracis*[a]			*B. cereus* G9241			*B. cereus* 03BB102		
	Gal #	[b][M + Na]$^+$	%[c]	Gal #	[b][M + Na]$^+$	%[c]	Gal#	[b][M + Na]$^+$	%[c]
One repeat[d]							1	812.3	68.9
	2	974.3	63.0				2	974.4	60.0
	3	1136.4	100.0	3	1136.4	100.0	3	1136.5	100.0
				4	1298.6	185.0	4	1298.5	155.6
							5	1460.7	97.8
Two repeats[d]							2	1583.7	86.7
	3	1745.6	3.3	3	1745.9	40.3			
	4	1907.6	13.2	4	1907.9	112.9			
	5	2069.7	22.0	5	2069.9	145.2	5	2069.8	24.4
	6	2231.7	16.5	6	2231.9	153.2	6	2231.9	26.7
				7	2394.0	129.0	7	2393.9	33.3
				8	2556.1	64.5	8	2556.0	35.6
							9	2718.0	24.4
							10	2880.1	9.3
Three repeats[d]	6	2842.8	1.6	6	2842.2	16.1			
	7	3002.8	5.5	7	3003.2	33.1			
	8	3164.8	4.4	8	3167.2	32.2			
	9	3327.8	1.5	9	3327.3	24.2			
				10	3492.2	17.7			
				11	3652.4	12.1			
Four repeats[d]							4	3126.2	11.6
							5	3288.2	13.6
							7	3613.4	5.6

The variation in galactose substitution of single and multiple repeating oligosaccharide units of the SCWP from strains of *B. anthracis*, and *B. cereus* strains G9241 and 03BB102 are compared.

[a]The SCWP-derived oligosaccharides from *B. anthracis* Ames, Sterne and Pasteur all give identical results.

[b]The observed ion mass.

[c]Ion intensity expressed relative to ion *m/z* 1136.4 (assigned as 100%). The spectrum of the *Bc*03BB87-derived oligosaccharides was virtually identical to that of *Bc*G9241.

[d]Fractions containing single, double and higher repeating units of the respective SCWPs were obtained by size exclusion chromatography on Bio-Gel P-2. Each repeating unit consists of three HexNAc residues and a variable number of Gal residues, e.g. the observed sodiated mass for one repeat with Gal #2 = 974.3; predicted mass = 973.87, calculated from the average incremental masses as described in Materials and methods.

indicates the presence of this repeating unit less one hexose (i.e. Gal). The next cluster of ions with mass 2232 represents the dimer of the hexasaccharide, and ions *m/z* 2070 and 1908 are, respectively, one and two Gal units less than the dimer. Ions were also observed for the trimer and higher oligomers with additional Gal differences. Interestingly, the SCWP from all pathogenic *B. cereus* and *B. anthracis* strains showed the presence of these same ions, indicating the presence of conserved structural features. However, the presence of additional ions with more, as well as less, Gal substitutions were also observed in the *B. cereus* SCWP, indicating additional heterogeneity of the secondary cell wall structures in these pathogenic *B. cereus* strains due to Gal substitution. The observed ions are listed in Table II and indicate that the repeating units of *B. cereus* G9241 and 03BB87 (which appear to yield identical spectra) have more variation in Gal substitution, with a tendency toward higher Gal substitution, than *B. anthracis* SCWP oligosaccharides. Since all of the Gal residues are terminally linked (shown by linkage analysis), the Gal heterogeneity is attributed to variable substitution onto the tri-aminosugar backbone. The *B. cereus* 03BB102 sample has an even greater variation in Gal substitution and may contain a more complex backbone.

Initial NMR comparison of the B. cereus *G9241 and* B. anthracis *SCWPs*

Initial NMR analysis of the *B. cereus* polymeric SCWPs obtained from Superose chromatography suggested considerably more complex or heterogeneous structures than *B. anthracis* SCWPs, and all of the *B. cereus* SCWPs displayed additional anomeric signals compared with the *B. anthracis* SCWPs (proton spectra are compared in Supplementary data, Figure S2). Closer examination of the anomeric region of these SCWPs by ^{1}H-^{13}C heteronuclear single quantum coherence spectroscopy (HSQC) analysis (Figure 3) revealed that many of these signals were conserved, although modified, between the two species, supporting the immunological and mass spectrometry data which indicated some degree of structural similarity. For reference, the glycosyl sequence of the *B. cereus* G9241 SCWP described in the present report is represented in Figure 4 together with SCWPs of the *B. anthracis* strains. The glycosyl sequence of the SCWPs from *B. anthracis* strains (i.e. Sterne 34F$_2$ and 7702, Pasteur, Ames) were previously determined and found to be identical (Choudhury et al. 2006).

NMR analyses of B. cereus *G9241 SCWPs and identification of glycosyl residues*

Commencing with the farthest downfield resonance (Figure 4D), the signal at δ_H 5.79 was assigned as the anomeric proton of residue **A**, subsequently identified as an α-Glc*p*NAc residue. The complete spin system was defined by ^{1}H-^{1}H correlation spectroscopy (COSY), total correlation spectroscopy (TOCSY), nuclear Overhauser effect spectroscopy (NOESY), ^{1}H-^{13}C HSQC and ^{1}H-^{13}HSQC-TOCSY analyses and the data are presented in Table III. Strong scalar coupling from protons H1–H5 in COSY and TOCSY analyses (Figure 5, Supplementary data, Figure S3), coupling from H4 to H6 in TOCSY and intraresidue NOEs between H2/H4 and H3/H5 indicated the *gluco* configuration and $^4C_1$ conformation for this residue, and the anomeric configuration was assigned from the $J_{C1,H1}$ coupling of 178.7 Hz. The proton assigned as H5 (δ 3.86) showed strong scalar coupling in TOCSY to protons assigned as H6 (δ 4.14/4.14); in the HSQC spectrum, the negative polarity of the H6/C6 connectivity indicated that these were indeed secondary protons, and the downfield shift of C6 (δ 68.0) indicated glycosidic linkage at the 6-position. The δ_C shifts of carbons C3 and C4 were also downfield from that expected (Lipkind et al. 1988) for unsubstituted carbons (Table III), suggesting that these positions were also glycosidically substituted. This system was further confirmed by HSQC-TOCSY analysis; in particular, connectivities were observed from H1/C1–H2/C2–H3/C3 (data not shown). A less abundant variant of residue **A** was assigned as residue **A′** (H1 δ 5.76, Figure 4 and Table III). This α-GlcNAc system also appeared to be tri-substituted based on the δ_C values at C3, C4 and C6. This set of α-GlcNAc signals (residues **A**/**A′**) are absent in the *B. anthracis* SCWP (Figure 4C).

Residues **B** and **C** were identified as α-Gal*p* residues that also occur in the *B. anthracis* SCWPs (Choudhury et al. 2006). However, in the *B. cereus* G9241 SCWP, each residue is further split into pairs of distinct yet very similar spin systems, presumably due to the additional structural heterogeneity in this SCWP. Residues **B** and **B′** (Figure 4 and Table III, anomeric protons δ_H 5.68 and 5.63) correspond to the α-Gal*p* residue having δ H1 5.64 in the *B. anthracis* SCWP (Choudhury et al. 2006). Residues **C** and **C′** (anomeric protons δ_H 5.55 and 5.52) correspond to the α-Gal*p* residue having δ H1 5.53 in the *B. anthracis* SCWP (Figure 4C). These residues (**B**/**B′** and **C**/**C′**) exist in different magnetic environments reflecting different points of attachment to the SCWP backbone as shown below. Additional data defining these α-Gal*p* residues are provided in the Supplementary data.

The cluster of signals around δ_H 5.22, assigned as residue **D**, is present in both the *B. anthracis* and *B. cereus* G9241 SCWPs and all resonances in this cluster arise from the anomeric proton of an α-Glc*p*NAc residue (Figure 4). Linkage (glycosidic substitution) at this residue is heterogeneous, contributing to the observed multiplicity of anomeric resonances in this group. In the *B. anthracis* structural study (Choudhury et al. 2006), the major system in this group, δ H1 5.22, was examined and identified as a 3,4,6-tri-substituted α-Glc*p*NAc residue. For the *B. cereus* G9241 SCWP, two of the major anomeric resonances in this cluster were examined and assigned as residues **D** and **D′** (δ H1 5.21 and 5.24; Table III). Downfield carbon shifts indicate that residue **D′** is substituted at positions O4 and O6 and that residue **D** is substituted at positions O3, O4 and O6. Both systems are

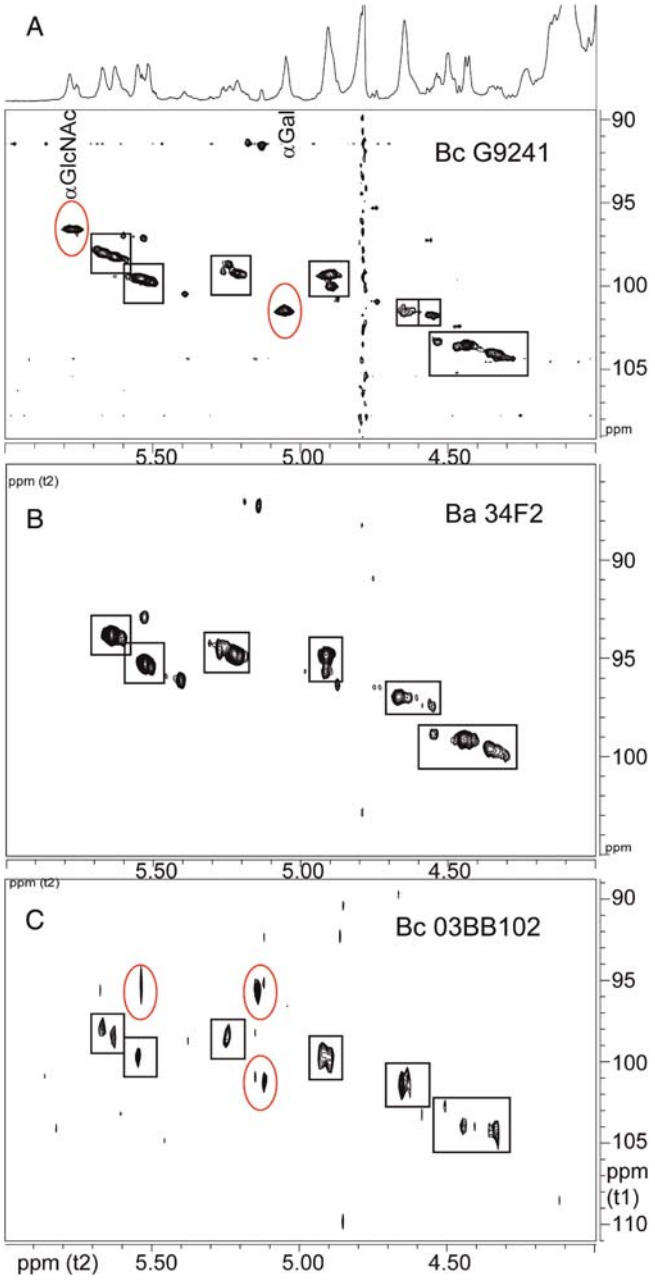

Fig. 3. Comparison of 600-MHz ^{1}H-^{13}C HSQC NMR spectra showing the anomeric regions of SCWP. (**A**) *B. cereus* G9241; (**B**) *B. anthracis* Sterne 34F$_2$; and (**C**) *B. cereus* 03BB102. The SCWP from *B. cereus* 03BB87 gives the same results as shown for *B. cereus* G9241. The SCWP from all the *B. anthracis* strains studied to date (Ames, Pasteur and several Sterne strains) have the same spectra as that shown in (B) (Sterne). The squares show conserved anomeric cross-peaks present in both *B. anthracis* and *B. cereus* strains, and ovals designate cross-peaks which are present in the *B. cereus* strains but are not found in *B. anthracis* strain SCWP.

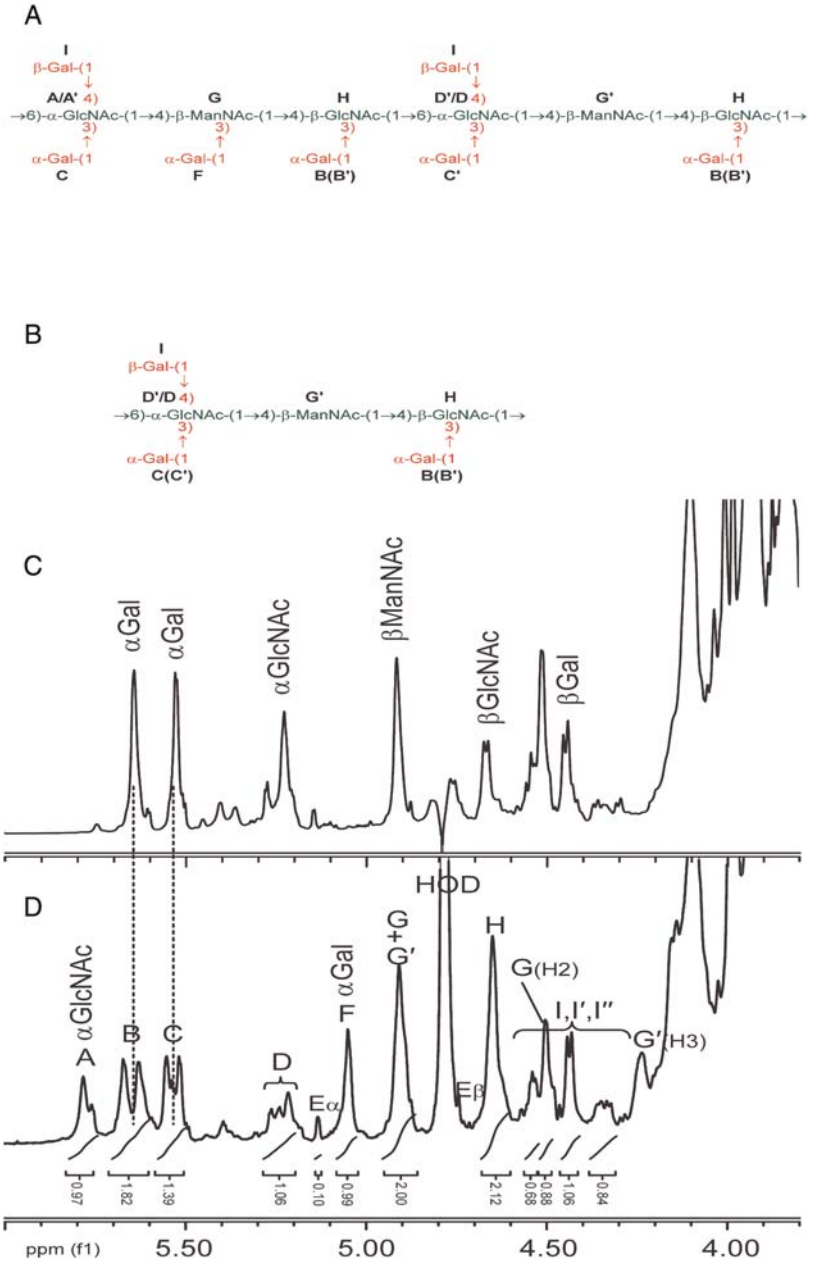

Fig. 4. Comparison of the repeating unit structures of the *Bacillus* SCWP and the anomeric regions of the 600-MHz proton NMR spectra for the SCWP. (**A**) The structure of the repeating unit of the *B. cereus* G9241 SCWP; (**B**) structure of the repeating unit from the *B. anthracis* SCWPs. The SCWP from all the *B. anthracis* strains studied to date (Ames, Pasteur and Sterne) have identical structures (Choudhury et al. 2006); (**C**) ^{1}H-spectrum, anomeric region, for *B. anthracis* Sterne 7702 SCWP; (**D**) spectrum for the *B. cereus* G9241 SCWP. The stoichiometry of the anomeric signals for the *B. cereus* G9241 strain is indicated. Residue **E**, anomeric signals attributed to the reducing-end GlcNAc residue. A small signal at approx. δ_H 5.4 arises from a contaminating α1 → 4 linked glucan.

characterized by strong COSY and TOCSY connectivities, and NOEs were observed between H1/H2, H2/H4 and H3/H5 (Figure 6 and Supplementary data, Figure S3), allowing assignment of the *gluco* configuration. The $J_{C1,H1}$ coupling constants (176.5–177.1 Hz) indicated the α-anomeric configuration. As discussed below, residues **A** and **D** are distinguished by the fact that they occupy distinct structural environments within the SCWP (Figure 4A), primarily reflecting differences in galactosyl side chain substitution at adjacent residues.

Residue **F** (δ H1 5.05) was identified as a terminal, unsubstituted α-Gal pyranose residue (Table III). As shown below, this residue is attached to a unique location in the *B. cereus* G9241 repeating unit and is absent in the *B. anthracis* SCWPs (Figure 4). Scalar connectivities observed during COSY analysis (not shown) allowed assignments of H1–H2

Table III. 800-MHz ^{1}H and ^{13}C NMR parameters observed for the SCWP released by HF treatment of *B. cereus* G9241 cell walls[a]

Compound glycose residue	$J_{C1, H1}$ (Hz)	δ_H ppm					
		δ_C ppm[b]					
		1	2	3	4	5	6
Native polysaccharide							
A →3,4,6)-α-D-Glc*p*NAc-(1→	178.7	5.79/96.61	4.15/52.79	3.99/75.56	4.07/77.70	3.86/69.98	4.14/4.14/68.0
A′ →3,4,6)-α-D-Glc*p*NAc-(1→	180.0	5.76/96.61	4.16/52.79	4.00/77.30	4.10/77.70	3.81/69.98	3.98/3.98/67.6
B α-D-Gal*p*-(1→	178.7	5.68/97.91	3.80/69.54	3.71/70.19	3.98/69.76	3.81/71.70	3.72/3.72/61.4
B′ α-D-Gal*p*-(1→	177.3	5.63/98.33	3.80/69.54	3.72/70.19	3.99/69.76	3.81/71.70	3.72/3.72/61.4
C α-D-Gal*p*-(1→	177.0	5.55/99.40	3.76/69.76	3.72/70.19	3.99/69.76	3.83/71.70	3.83/3.74/61.6
C′ α-D-Gal*p*-(1→	177.1	5.52/99.62	3.76/69.76	3.71/70.19	3.98/69.76	3.86/71.70	3.83/3.74/61.6
D′ →4,6)-α-D-Glc*p*NAc-(1→	176.5	5.24/98.76	3.91/53.86	3.86/71.69	3.63/79.86 (D′) and 3.72/79.63 (D″)	3.77/71.69	3.95/3.93/67.6
D →3,4,6)-α-D-Glc*p*NAc-(1→	177.0	5.21/99.19	4.08/53.43	4.01/75.72	4.03/77.06	3.96/71.47	4.14/4.13/67.4
F α-D-Gal*p*-(1→	172.6	5.05/101.56	3.77/68.68	3.65/70.19	3.93/69.97	4.15–4.20/72.13	3.73/3.73/62.46
G →3,4)-β-D-Man*p*NAc-(1→	165.1	4.91/99.40	4.65/54.51	4.24/80.28	4.10/77.27	3.52/75.56	3.89/3.91/60.7
G′ →4)-β-D-Man*p*NAc-(1→	165.0	4.90/100.04	4.50/54.51	4.05–4.10/73.41	3.67–3.73/76.20	3.51/75.35	3.91/3.82/61.2
H →3,4)-β-D-Glc*p*NAc-(1→	159.4	4.65/101.54	3.90–3.91/55.15	3.90/75.98	4.10/77.31	3.52/75.99	3.74/3.92/60.7
I[c] β-D-Gal*p*-(1→	163.7	4.44/103.48	3.54/71.70	3.64/73.30	3.94/69.33	3.66/76.21	3.75/3.82/61.8

The intact polysaccharide was purified by Superose size exclusion chromatography and subjected to NMR analysis.
[a]800 MHz spectra measured at 25°C in D_2O relative to internal DSS (δ_H 0.00 ppm).
[b]Carbon δ_C obtained from ^{1}H-^{13}C HSQC spectra; carbonyl δ_C from the HMBC spectra.
[c]Additional heterogeneity exists for residue **I**; the major spin system is listed here, and less abundant systems (**I′**, **I″**, etc.) are listed in Supplementary data.
Additional signals. Pyruvate: C1, (C = O) δ 177.04, (C2) δ 100.70, (C3) CH_3 δ 25.29, CH_3 δ 1.55; *N*-acetyl: βGlcNAc, C = O δ 174.46, CH_3 δ 22.93, CH_3 δ 2.08; αGlcNAc, C = O δ 176.20, CH_3 δ 20.99, CH_3 δ 2.08; βManNAc, C = O δ 175.97, CH_3 δ 22.93, CH_3 δ 2.03; residue **E** (α-reducing end): →3,6,4)-α-D-Glc*p*NAc, H1/C1 δ 5.13/91.67 ($J_{C1,H1}$ 171.1 Hz), H2/C2 δ 4.06/53.5, H3 δ 3.94, H4 δ 3.83, H5 δ 3.75, H6 not assigned; (β-reducing end): H1/C1 δ 4.74/95.32, H2/C2 δ 3.79/56.12, H3/H4/H5 = δ 4.07/3.87/3.52; H6 not assigned.

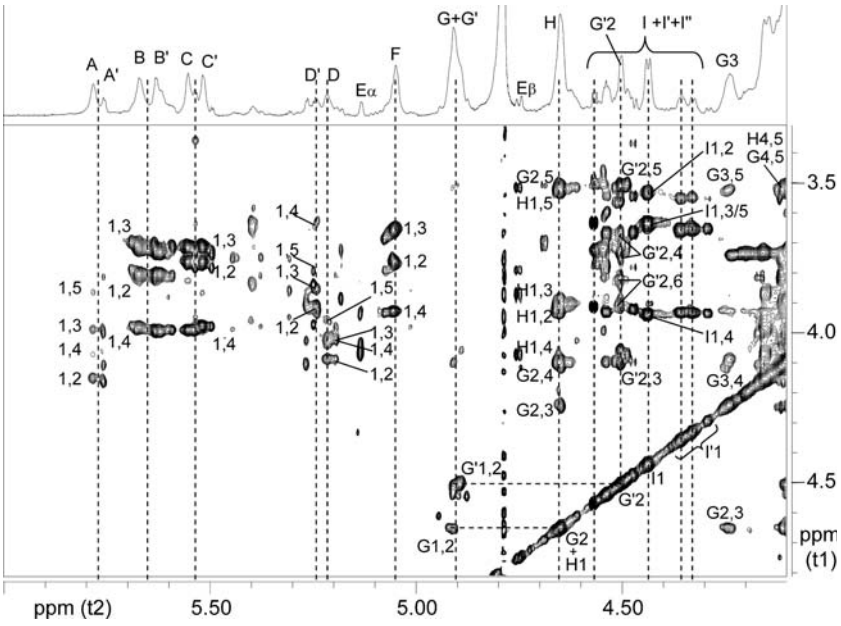

Fig. 5. Partial 800-MHz ^{1}H-^{1}H TOCSY spectrum of the *B. cereus* G9241 secondary cell wall SCWP. Scalar correlations involving the anomeric protons of residues **A** through **I** are labeled; correlations involving H2 of ManNAc (residues **G** and **G′**) are also labeled. Additional ring proton scalar couplings are shown in Supplementary data.

(δ 3.77), H2–H3 (δ 3.65) and H3–H4 (δ 3.93). Magnetization transfer beyond H4 was not observed during TOCSY/COSY analyses, consistent with the *galacto* configuration. Strong NOEs between H3/H4 and from H4 to a proton at δ 4.15–4.20 suggested the latter as H5, and strong scalar coupling in TOCSY/COSY between H5 and proton(s) at δ 3.730 (Supplementary data, Figure S3), allowed assignment of the latter to H6. Further confirmation of this system was obtained from an HSQC-TOCSY analysis which showed connectivity between positions H6/C6 to H5/C5 (δ_H/δ_C 3.73/3.73/62.46 to

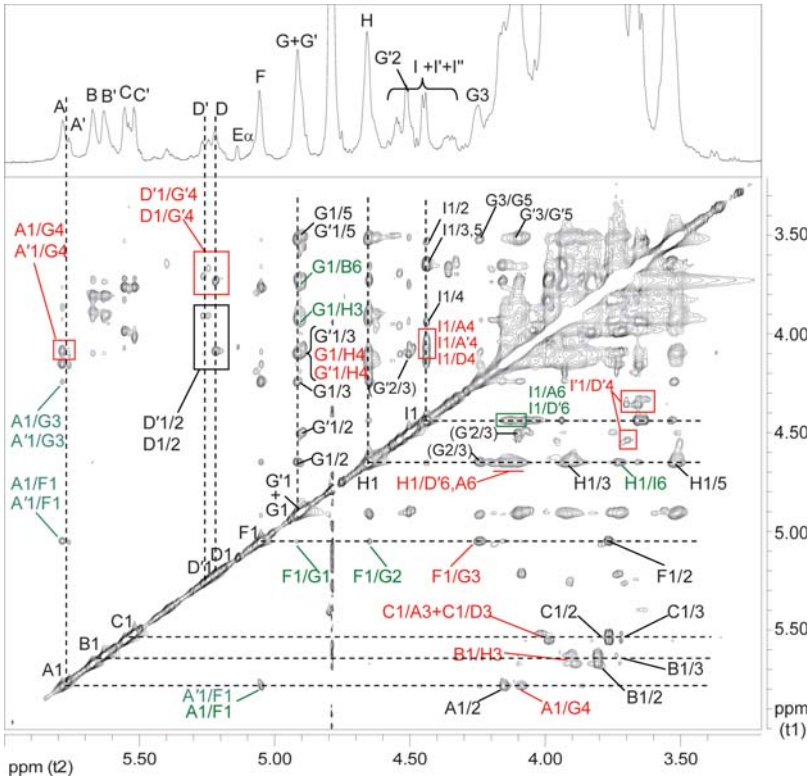

Fig. 6. Partial 800-MHz ^{1}H-^{1}H NOESY spectrum of the *B. cereus* G9241 secondary cell wall SCWP. Interresidue NOEs not involving linkage are labeled in green and interresidue NOEs at linkage are labeled in red text. Additional NOEs involving intraresidue ring protons are shown in Supplementary data.

4.15–4.20/72.13). A comparison of the HSQC spectra for the *B. cereus* and *B. anthracis* SCWPs shows that all δ_H/δ_C resonances comprising this spin system are notably absent in the latter (Figure 7).

Residue **G** consisted of two major glycosyl systems (**G** + **G′**) which could be deduced from the COSY, TOCSY and NOESY analyses. Although the anomeric signals were virtually identical, the δ_H and δ_C at positions 2, 3 and 4 differed, reflecting differences in glycosidic substitution (Figure 4, Table III). Residue **G** (H1 δ 4.91) was identified as β-Man*p*NAc, based on unresolved $J_{H1,H1}$, the downfield resonance of H2 proton (δ 4.65) and weak or undetectable scalar coupling beyond H1/H2. Scalar couplings in COSY did allow assignment of protons H2 and H3 (δ 4.24). In the TOCSY analysis, starting from H2, scalar coupling was observed with protons H2, H3 and two other protons subsequently assigned H4 and H5 (Figure 5). Further TOCSY couplings (Supplementary data, Figure S3) between H4/H5 (δ 4.10/3.52) and H5/H6 (δ 3.52/3.89–3.91) allowed initial assignment of all ring positions. These assignments were confirmed by NOEs for protons H1/H2, H1/H3, H1/H5 and H3/H5 (Figure 6) and supported by characteristic carbon shifts (Lipkind et al. 1988) at positions 2, 5 and 6. Subsequently, intraresidue heteronuclear multiple bond coherence spectroscopy (HMBC) correlations were observed between atoms H1-C2, H1-C3 and H2-C3, supporting these assignments (Figure 8). The observed NOEs involving H1, the characteristic C5 shift (δ_C 75.56) and the $J_{C1,H1}$ coupling (165.1 Hz) were indicative of the β-anomeric configuration. A downfield shift in δ_C values indicated that this residue was glycosidically substituted at positions O3 and O4. The variant residue **G′** (H1 4.90) was also identified as β-Man*p*NAc, however, substituted only at position O4 (δ_C 76.20). Intraresidue NOEs were observed between H1/H2, H1/H3, H1/H5 and H3/H5 (Figure 6). Comparison of the NMR data for these β-ManNAc residues in this *B. cereus* SCWP, with the *B. anthracis* SCWPs, shows that the latter contain only the mono-substituted Man*p*NAc (**G′**), lacking the di-substituted (branch point) Man*p*NAc (**G**) residue.

Residue **H** (H1 δ 4.65) was identified as β-Glc*p*NAc, based on the strong COSY and TOCSY scalar coupling throughout the ring, NOEs observed between H1/H3/H5 and H2/H4 (Supplementary data, Figure S3) and the $J_{C1,H1}$ value (159.4 Hz). This residue is glycosidically substituted at positions O3 and O4 based on the δ_C values (Table III). This di-substituted β-GlcNAc residue also occurs in the *B. anthracis* SCWPs (Choudhury et al. 2006) at δ H1 4.67 (Figure 4B and D).

The majority of signals ranging from δ_H 4.57 to 4.29 were readily assigned as anomeric protons of terminal, unsubstituted β-Gal*p* residues (residue **I** + **I′** + **I″** series) based on their COSY, TOCSY, NOESY and HSQC characteristics. The pattern of anomeric protons in this region is virtually identical to those in the *B. anthracis* SCWPs (Figure 4), suggesting that substitution by β-Gal residues occurs at identical locations in both SCWPs. The exception to these assignments was a single proton at δ_H 4.502, readily identified as H2 of residue **G′**. This H2 signal also occurs in the *B. anthracis* SCWPs.

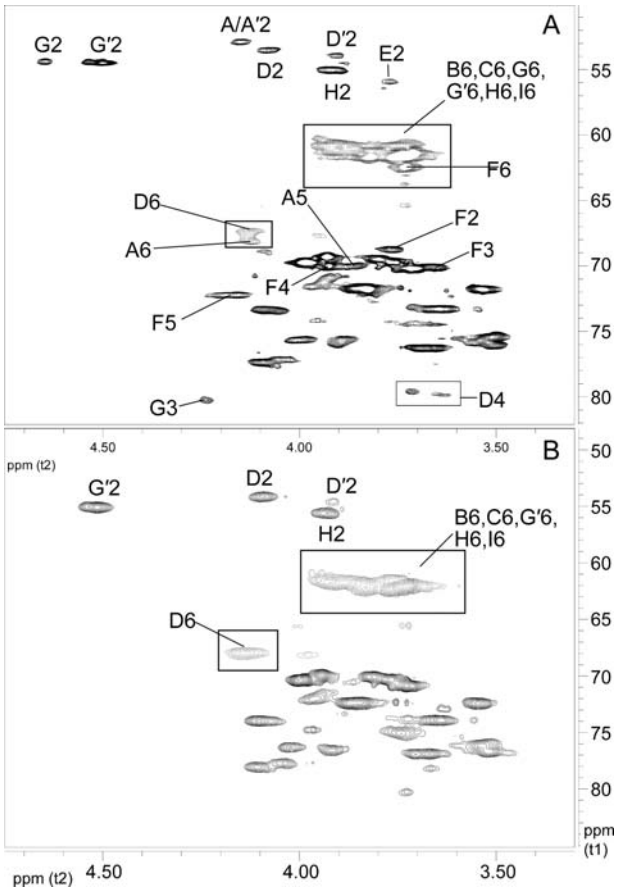

Fig. 7. Partial 600-MHz ^{1}H-^{13}C HSQC spectral comparison of the pathogenic *B. cereus* and *B. anthracis* secondary cell wall SCWPs. The ring proton regions are compared for (**A**) *B. cereus* G9241 SCWP ^{1}H-^{13}C HSQC ring proton region; (**B**) *B. anthracis* Sterne 34F$_2$ SCWP ^{1}H-^{13}C HSQC ring proton region. The *B. cereus* G9241 spectrum is virtually identical with that of *B. anthracis* Sterne, apart from the appearance of new signals present in the *B. cereus* G9241, including variant forms of residues **G** and **D** (yielding **G** + **G′** and **A**/**A′**) and six new signals arising from residue **F** (α-Gal*p*).

As discussed below, the overwhelming majority of the β-Gal residues were found to be attached to a specific location in the repeating unit backbone of the SCWP. The major β-Gal system was assigned as residue **I** (H1 δ_H 4.44, $J_{1,2}$ 7.4 Hz; Table III).

Glycosyl arrangement and sequence as determined from interresidue HMBC and NOE analyses

Both residues **A** and **A′** (α-GlcNAc) showed a strong NOE (Figure 6) from their respective H1 protons (δ 5.79 and 5.76) to a proton at δ 4.10 identified as H4 of residue **G** (ManNAc), suggesting that residues **A**/**A′** are linked α(1 → 4) to residue **G**. Both residues **A** and **A′** also exhibited a less intense NOE (Figure 6) from their H1 protons to a proton at δ 4.24, the H3 proton of **G** and an intense NOE from H1 to a proton at δ 5.05, the anomeric proton of α-Gal residue **F**. The resulting structural arrangement **A**/**A′**α(1 → 4)[**F**α(1 → 3)]**G** was substantiated by a strong NOE between H1 of residue **F** (δ 5.05) and H3 of ManNAc residue **G** (δ 4.24) and the fact that no NOE was observed between H1 of **F** and H4 of **G**. Conclusive evidence for these linkages was obtained from interresidue HMBC correlations (Figure 8), from the H4 proton of residue **G** to the anomeric carbon of **A** (**G**4-**A**1), and between **G**3-**F**1 (Supplementary data, Figure S4).

The group of anomeric resonances assigned as residue **D**/**D′** (α-GlcNAc) showed strong interresidue NOEs from their anomeric protons to a family of protons identified as H4 of ManNAc residue **G′** (Figure 6). Residue **D**, the major component, showed a strong interresidue NOE between its anomeric proton at δ 5.21 and a proton at δ 3.73, H4 of **G′**. Other members of the residue **D** family, for instance, **D′**, showed a similar interresidue NOE from the **D′** anomeric (δ 5.24) to a proton at δ 3.67, also identified as part of the family of resonances belonging to H4 of the **G′** ManNAc residue. These NOEs suggest that the glycosyl sequence **D**/**D′**α(1 → 4)**G′** exists in the *B. cereus* G9241 SCWP, identical to the glycosyl sequence and residues present in the *B. anthracis* SCWPs (Choudhury et al. 2006) in which the ManNAc residue is substituted only at position O4, lacking Gal substitution at O3. In the *B. cereus* G9241 SCWP, ∼50% of these ManNAc residues are substituted by α-Gal at O3, yielding the sequence **A**/**A′**α(1 → 4)[**F**α(1 → 3)]**G** discussed above, in addition to the **D**/**D′**α(1 → 4)**G′** sequence. Additional evidence for the **D**/**D′**α(1 → 4)**G′** linkage was obtained from an interresidue HMBC correlation, between the H4 protons of **G′** and the anomeric carbon of **D**/**D′** (**G′**4-**D**1/**D′**1; Figure 8 and Supplementary data, Figure S4). The signal heterogeneity at proton H4 of **G′** can probably be attributed to the heterogeneity of its glycosidic substituent (residue **D**/**D′**) which appears to be one of the main sources of structural heterogeneity in these SCWPs, reflecting differences in Gal substitution at the **D** residue.

In the *B. cereus* G9241 SCWP, both ManNAc residues (**G** and **G′**) exhibited strong interresidue NOEs from their respective anomeric protons to a proton at δ 4.10, identified as H4 proton of β-GlcNAc (residue **H**; Figure 6). These results indicate that all β-ManNAc residues are linked 1 → 4 to the β-GlcNAc residue, in both *B. cereus* G9241 and *B. anthracis* SCWPs, irrespective of their substitution by α-Gal. This linkage, **G**/**G′**β(1 → 4)**H** was substantiated by three-bond interresidue HMBC connectivities between H1 of β-ManNAc and C4 of β-GlcNAc, and between H4 of β-GlcNAc (δ 4.10) and C1 of β-ManNAc (δ_C **G** 99.4; δ_C **G′** 100.0), (labeled **G′** 1/**G**1-**H**4 and **H**4-**G′**1/**G**1, respectively; Figure 8).

Several NOEs were observed (Figure 8) from the anomeric proton of residue **H** (δ 4.65, β-GlcNAc). In addition to intraresidue NOEs discussed above, the significant interresidue NOEs detected were between H1 of residue **H** and the H6 protons of residues **A** and **D**, providing evidence for the β(1 → 6) linkage connecting these two GlcNAc residues. This linkage was substantiated by an interresidue HMBC correlation **H**1-**A**6/**D**6 (Figure 8). An additional interresidue NOE was observed between the anomeric proton of residue **H** and a proton at δ 4.44, the anomeric proton of β-Gal (residue **I**).

Further evidence for the attachment of β-Gal (residue **I**) to position O4 of the α-GlcNAc residues (**A**/**D**) was provided by interresidue NOEs between the β-Gal anomeric proton (δ 4.44) and protons at δ 4.03–4.10, which correspond to the H4

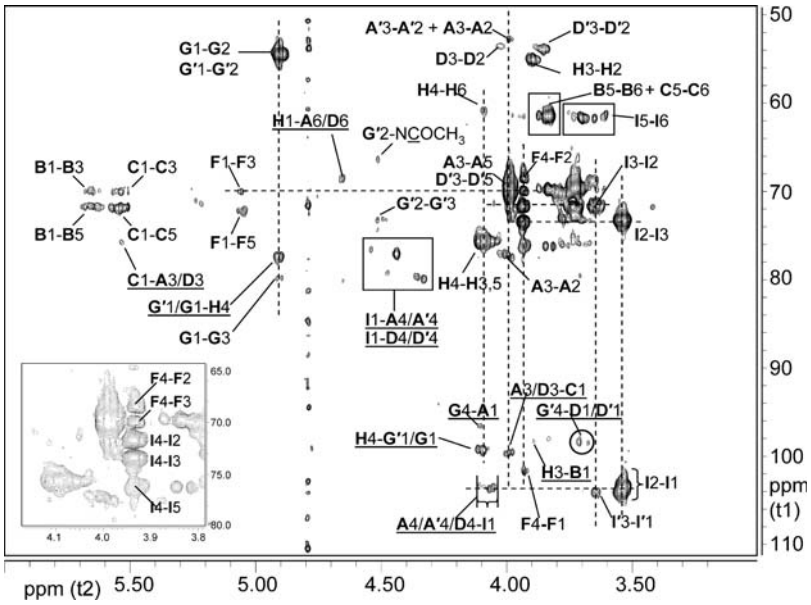

Fig. 8. Partial 800-MHz ^{1}H-^{13}C HMBC spectrum of the *B. cereus* G9241 SCWP. Interresidue correlations defining all glycosidic linkages are underlined. Residues are in bold type and all connectivities are listed in the sequence: "proton-carbon", e.g. **G′**1/**G**1-**H**4 designates a three-bond interresidue correlation between the anomeric proton of residue **G** and C4 of residue **H**, and the identical correlation between residues **G′** and **H**. An expanded region showing weak interresidue HMBC correlations is shown in the Supplementary data.

protons of α-GlcNAc residues **A**/**A′** and **D** (Figure 6). This location for β-Gal in 1 → 4 linkage was conclusively shown by interresidue HMBC connectivities between H4 of α-GlcNAc residues **A**, **A′** and **D** (δ 4.03–4.10) and C1 of β-Gal (δ_C 103.48). An interresidue NOE between the β-Gal anomeric proton and the H6 protons of α-GlcNAc (**A**/**D**) was observed and is consistent with rotation about the 1 → 6 linkage. As is the case for the *B. anthracis* SCWP, this β-Gal location constitutes the primary site of β-Gal attachment in the *B. cereus* SCWP. The anomeric protons of the minor systems **I′** and **I″** also show interresidue NOEs to H4 of residue **D′**.

Residues **B** and **B′**, the α-Gal residues having H1 at δ 5.68 and 5.63, show intense interresidue NOEs to a proton at δ_H 3.90 (Figure 6), identified unambiguously as H3 of β-GlcNAc (residue **H**). These results are consistent with the previously published assignment of this α-Gal residue in the *B. anthracis* SCWPs. The reason for the observed splitting of **B** residue anomeric proton into two signals (**B** and **B′**) is not entirely clear, aside from the obvious fact that slightly different magnetic environments must exist for **B** and **B′**. We propose that the attachment of an additional α-Gal onto ∼50% of the ManNAc residues creates two distinct magnetic environments and influences proton shielding to various extents at adjacent residues.

Anomeric protons at δ 5.55 and 5.52, designated as α-Gal residues **C** and **C′**, exhibited strong NOEs to protons at δ 3.99 and 4.01, identified as the H3 protons of α-GlcNAc residues **A** and **D**, respectively. This indicates that Gal residues are attached in α(1 → 3) linkage to the backbone α-GlcNAc residue, a structural feature that was also present in the *B. anthracis* SCWP. In the case of the *B. cereus* G9241 SCWP, the **C** α-Gal residues are again split into two anomeric signals; all the remaining ring positions have essentially identical δ_C and δ_H values (Table III). The residue designated **C** is essentially restricted to attachment at residue **A**, and residue **C′** is linked exclusively to residue **D** (Figure 4A).

Residue stoichiometry and other structural features

Assuming a molar equivalency in signal response, the molecular size of the SCWP was estimated by comparing the areas of the anomeric signals attributed to the reducing-end residue with any of the backbone hexosamine residues in the repeat unit, e.g. ManNAc (**G** + **G′**). Residue **Eα**/**β** was assigned as a reducing-end GlcNAc residue based on δ_H and δ_C values (Figure 4 and footnote in Table III). This assignment was also consistent with direct phosphorus observed in NMR analysis, which indicated that the SCWP was devoid of phosphate, suggesting a free reducing-end glycosyl residue. The **E**:**G** area ratio was 1:10, and since two **G** residues occur per every di-repeat, this yields an estimated mass of ∼12 kDa, consistent with the size exclusion chromatographic results for the *B. cereus* G9241 SCWP.

Pyruvate was identified in the SCWPs from all three pathogenic *B. cereus* strains (G9241, 03BB87 and 03BB102) as well as the *B. anthracis* strains (Sterne 34F_2, 7702) (Supplementary data, Figure S2). This substituent was defined by HMBC correlations between the methyl group protons to pyruvate carbons-1 and -2 (Table III and Supplementary data, Figure S5). Due to the low abundance of this moiety, HMBC connectivities between sugar ring protons and C2 of pyruvate could not be detected, so the pyruvate moiety could not be localized to a particular residue. The area of the methyl proton signal to ManNAc anomeric proton is 0.26:1.00, and since the former represents three protons, the effective ratio of a single pyruvate methyl group per ManNAc residue is calculated to be

0.09:1.0 equivalent to ~0.9 molecules of pyruvate per SCWP molecule (i.e. per every 10 ManNAc residues).

The three major acetate signals in the *B. cereus* G9241 SCWP arise from *N*-acetylation, and HMBC and NOE connectivities allow these moieties to be assigned to their respective residues (Table III). A very weak signal was also detected in the 800 MHz HSQC spectrum, characteristic of a ring proton/carbon bearing an *O*-acetylation site (δ_H/δ_C 5.10/74.49). The low intensity of this signal precluded localization to a specific glycosyl residue and suggested a stoichiometry comparable to that of pyruvate. Both *O*-acetylation and pyruvylation have been implicated as components of the binding site recognized by SLH-domain proteins (Kern et al. 2010).

Discussion

A recent review by Schäffer and Messner (2005) addressed the structures of nonclassical SCWP from bacilli. The general structural feature for all of these SCWPs is that they have repeating oligosaccharide units that contain aminoglycosyl residues and that at least one of these residues has the *manno* configuration and a second has the *gluco* configuration. This general structural theme was also present in the SCWP structures of *B. anthracis*, *B. cereus* ATCC 10987 and *B. cereus* ATCC 14579 (Choudhury et al. 2006; Leoff, Choudhury et al. 2008). These reported structures were consistently composed of an aminoglycosyl trisaccharide backbone. While it has been reported (Mesnage et al. 2000; Kern et al. 2010) that these SCWPs are involved in anchoring and/or targeting proteins to the cell surface, including the S-layer proteins, it is not known whether they have essential functions for viability or virulence. As a preliminary to further functional analysis, in this paper we immunochemically investigated the structural relatedness between the SCWP from *B. anthracis* with the SCWP from pathogenic *B. cereus* strains. In addition, we elucidated the complete SCWP glycosyl structure from strain *B. cereus* G9241, a strain that was isolated from patient suffering from severe pneumonia.

We previously showed that the glycosyl structure of the SCWP from *B. anthracis* consists of a repeating →6)-α-GlcNAc-(1 → 4)-β-ManNAc-(1 → 4)-β-GlcNAc-(1→ trisaccharide backbone in which the α-GlcNAc residue is substituted with α-Gal and β-Gal at the 3- and 4-positions, respectively, and the β-GlcNAc residue is substituted with α-Gal at the 3-position (Choudhury et al. 2006). In this report, we show that the structure of the SCWP from *B. cereus* G9241 differs from the *B. anthracis* structure in that it has an additional α-Gal residue attached to the 3-position of the backbone ManNAc residue and that this substitution is nonstoichiometric, giving rise to considerable structural heterogeneity of the SWCP. In the *B. cereus* G9241 SCWP, ~50% of the backbone ManNAc residues carry this 3-*O*-α-Gal substituent, based on integration of anomeric signals (Figure 4). Comparison of the *B. cereus* G9241 and *B. anthracis* SWCPs with those of *B. cereus* 03BB87 and 03BB102 by NMR and MS analyses showed that the latter two SCWPs also vary in structure from that of *B. anthracis* in their galactosylation pattern. The data indicate that *B. cereus* 03BB87 SCWP has an identical structure to that of *B. cereus* G9241 and that strain *B. cereus* 03BB102 SCWP is galactosylated to an even greater extent, with additional structural heterogeneity than either *B. cereus* G9241 or *B. anthracis* SCWPs.

The extent of structural heterogeneity of the strain G9241 SCWP can further be detailed by integration of the anomeric resonances shown in Figure 4. The backbone HexNAc residues exist in a 1:1:1 ratio for α-GlcNAc:β-ManNAc:β-GlcNAc, i.e. $(\mathbf{A}+\mathbf{A'}+\mathbf{D}+\mathbf{D'}):(\mathbf{G}+\mathbf{G'}):\mathbf{H}$. The overall ratio of total Gal to HexNAc indicates approximately seven Gal residues per each di-repeat unit, a value which is slightly higher than that observed for the *B. anthracis* SCWPs (six Gal per di-repeat). This increase is attributed to the attachment of the additional α-Gal (residue **F**) to roughly half of the backbone ManNAc residues in the *B. cereus* G9241 SCWPs. These estimates are also consistent with the mass spectra analysis, which suggested maxima of about six Gal per di-repeat for *B. anthracis* and seven to eight Gal per di-repeat for *B. cereus* G9241 and 03BB87 (Figure 2, Table II). The presence of ions representing eight Gal per di-repeat for G9241 and 03BB87 SCWPs could arise from contiguous repeats in which both ManNAc residues are substituted with Gal. There is every indication that approximately one out of every two ManNAc residues is substituted by α-Gal, e.g. the ratio of the new Gal residue to ManNAc anomeric signals, i.e. $\mathbf{F}:(\mathbf{G}+\mathbf{G'})$ is 0.99:2.0. However, the distribution of these two forms of repeating unit, throughout the polymer (i.e. random, alternating, etc.) cannot be determined from these data. The situation with *B. cereus* strain 03BB102 is more complex, since mass spectra indicate up to 10 Gal per di-repeat and the NMR spectra show additional complexity. All of the SCWPs from all strains examined to date display nonstoichiometric NMR signals for pyruvate acetal (e.g. Supplementary data, Figure S2, and Table III), at an abundance of roughly 0.9 residues per polysaccharide molecule. The chromatographic profiles (Supplementary data, Figure S1) indicate that SCWPs released by HF treatment are polysaccharides of notable size, with MMs around 12–20 kDa. Using mass spectral analysis, Kern et al. (2010) suggested that pyruvylation may be restricted to the nonreducing end of the *B. anthracis* SCWP, where it could help facilitate binding to the SLH domain of the S-layer glycoproteins. As represented in Figure 4, virtually every backbone residue is substituted with at least one Gal side chain. Such polysaccharides could align into an ordered surface layer, providing the necessary foundation for S-layer adhesion to the pyruvylated nonreducing terminal.

Our structural work thus confirms our previous suggestion that SCWP structures of these *B. cereus* strains associated with severe disease are similar to that of *B. anthracis*. In fact, the data support the conclusion that all three structures contain the same →6)-α-GlcNAc-(1 → 4)-β-ManNAc-(1 → 4)-β-GlcNAc-(→ repeating trisaccharide backbone and differ with respect to substitution of this backbone with terminal Gal residues, with greater substitution occurring in the *B. cereus* G9241 and *B. cereus* 03BB87 SCWPs by the additional α-Gal on the ManNAc residue. The *B. cereus* 03BB102 SCWP displays still greater Gal substitution; however, other structural differences may also exist and the 03BB102 polysaccharide requires further characterization.

Immunochemical analysis showed that approximately half of the *B. cereus* Clade 1 strains (including *B. anthracis* strains) reacted positively with the anti-$SCWP_{Ba}$ antiserum, which is consistent with our results showing structural similarities in the SCWP of these *B. cereus* strains with that from *B. anthracis*. In fact, within the group of *B. cereus* Clade 1 strains tested, it is notable that with the exception of two strains, all *B. cereus* isolated from patients with severe infections such as pneumonia showed cross-reactivity with the anti-$SCWP_{Ba}$ antiserum. Cross-reactivity was not detected between the anti-HF-$PS_{B.anthracis}$ antiserum and any of the *B. cereus* Clade 2 strains, including those strains isolated from patients suffering from pneumonia.

The three pathogenic *B. cereus* strains examined here not only have SCWP structures similar to that of *B. anthracis*, but also harbor *B. anthracis* virulence plamids and/or genes (Hoffmaster et al. 2004, 2008). At this time, it is not known whether these genetic similarities are responsible for the severe or fatal illnesses caused by these *B. cereus* strains, or whether the SCWP plays a role (directly/indirectly) in their pathogenicity. For example, it may be that the SCWP structure contributes to or defines a bacterial cell surface that allows *B. cereus* strains to acquire one or both of the *B. anthracis* virulence plasmids or the pathogenicity island of pXO1. Case reports about anthrax infections in great apes at the Côte d'Ivoire and in Cameroon could provide some clarification since these isolates from primates showed very interesting parallels to the *B. cereus* strains in this study. Initial investigations of the bacterial strains isolated from four chimpanzees and one gorilla suggested that they presumably died of anthrax even though microbiological features, i.e. high motility, resistance to gamma-phages and penicillin G, would suggest that the isolates are not *B. anthracis* species (Klee et al. 2006). However, Southern blot analysis and reverse transcriptase–polymerase chain reaction confirmed the presence of *B. anthracis* virulence plasmids pXO1 and pXO2. MLST analysis classified these strains as sequence type 1 and 2, the same sequence type as 'classic' *B. anthracis* strains (Klee et al. 2006) and the recent sequencing of a genome led to their suggested classification as *B. cereus* variety (var.) anthracis (Klee et al. 2010). The analysis of the SCWP from these newly identified *B. cereus* var. anthracis strains will further test the possibility of a common structural pattern in the SCWPs of *B. anthracis* and other Clade 1 strains that cause severe and fatal infections.

Materials and methods

Bacillus *strains and clinical isolates*

B. anthracis strains 7702 and Sterne $34F_2$, *B. cereus* G9241, *B. cereus* 03BB87, *B. cereus* 03BB102 and *B. cereus* ATCC 14579 were provided from the Centers for Disease Control and Prevention culture collection. Cultures were grown as described previously (Choudhury et al. 2006; Leoff et al. 2009).

Twenty-five clinical isolates of *B. cereus* were included in this study (see Table I) for immunofluorescence labeling with anti-SCWP antiserum raised in rabbits against HF-PS-KLH conjugate antigen from *B. anthracis* (Leoff et al. 2009). All isolates were of clinical origin and associated with gastrointestinal, fatal pneumonia or other illness. MLSTs, subtypes and clades associated with these isolates were previously reported by Hoffmaster et al. (2008). Thirteen isolates included in the current study are phylogenetically within Clade 1 and 14 isolates within Clade 2 of the *B. cereus* group of strains (Hoffmaster et al. 2008). Positive controls used were *B. anthracis* Sterne $34F_2$ and *B. cereus* G9241, and as negative control the *B. cereus*-type strain ATCC 14579 (Leoff et al. 2009).

Immunofluorescence

Control strains were stored at 4°C as spore suspensions in water. All other strains were kept at −70°C as spore suspensions in water containing 25% glycerol. Fifty microliters of vegetative cells grown overnight under shaking in heart infusion broth were added to 50 µL of a 1:10 dilution of anti-$SCWP_{Ba}$ antisera and incubated at 37°C for 10 min. Cells were recovered by centrifugation at 14,000 × *g* for 3 min and washed twice with 1 mL of 10 mM phosphate-buffered saline/0.3%Tween 20, pH 7.2 (PBST). After the final wash, 50 µL of supernatant was left to resuspend the cells and 2 µL of fluorescently labeled goat antirabbit conjugate (0.2 mg/mL; Invitrogen, Carlsbad, CA) was added and incubated at 37°C for 10 min. The reaction mixture was diluted with 1 mL of PBST and centrifuged at 14,000 × *g* for 3 min. This wash was repeated using deionized water instead of PBST. Following centrifugation, the supernatant was removed leaving behind 100 µL of water. The pellet was resuspended in residual fluid and 2 µL of the suspension was placed on a 12-well Teflon-coated microscope slide (Cle-Line/Erie Scientific Co., Portsmouth, NH) and allowed to air-dry for ∼10 min. One drop of DAKO faramount aqueous medium (DAKO Co., Carpinteria, CA) and a cover slip were applied to the slide. Labeled cells were visualized on a UV microscope using a 100× objective. Cells which exhibited bright green fluorescence were scored positive, whereas negative reactions lacked fluorescence.

Isolation of cell walls

Cell walls were prepared from cultured cells as previously described (Choudhury et al. 2006; Leoff et al. 2009), following a modified procedure (Brown 1973). The procedure yielded ∼30–70 mg of cell walls per 100 mL of cultured cells.

Isolation and purification of SCWPs

Cell wall preparations from *B. cereus* G9241, *B. cereus* 03BB87, *B. cereus* 03BB102, *B. cereus* ATCC 14579 and *B. anthracis* Sterne $34F_2$ and Sterne 7702 were treated with 48% aqueous hydrogen fluoride (HF) at 4°C for 48 h. The reaction mixtures were rotated slowly in an end-over end mixer to assist solubilization of the cell wall material. The reaction mixtures were then adjusted to pH 6.0 by rapidly transferring the mixtures directly into a predetermined amount of ammonium hydroxide solution (20%, v/v) precooled to −20° C. The solutions were then dialyzed at 4°C vs. deionized water for 3 days using 1000 molecular weight cut off dialysis tubing. Dialysates were concentrated by centrifugal vacuum

evaporation and then subjected to ultracentrifugation (100,000 × *g*; 4°C, 4 h) to remove HF-insoluble material, yielding a supernatant containing the solubilized SCWPs (crude SCWP preparation). The HF-insoluble residue consisted of peptidoglycan fragments and protein (amino acids) as determined by gas–liquid chromatography-mass spectrometry (GC-MS) analysis of the heptafluorobutyrate esters and trimethylsilyl (TMS) methyl glycosides.

Crude SCWP was dissolved in water, filtered (0.45 µm cellulose acetate), then purified by SEC on Superose-12 column eluted in 50 mM ammonium acetate. The eluant was monitored by UV absorbance (215 nm) and refractive index, and fractions containing the SCWP were identified by glycosyl analysis. The SCWP fractions were pooled, lyophilized and used for structural and immunological analyses. The yield was typically 5 mg of purified SCWPs per 40 mg of cell wall material.

Isolation of SCWP-derived oligosaccharides

Our initial attempts to isolate the intact SCWP by release with HF-treatment yielded, in addition to a polymeric fraction, a lower MW fraction which could be isolated by SEC on Bio-Gel P-2 column. Chromatography on Bio-Gel was performed as described (Choudhury et al. 2006), and the oligosaccharide fractions were analyzed by glycosyl analysis and mass spectrometry.

Glycosyl analyses

Carbohydrate compositions of the SCWP and derived fractions were determined by preparing the TMS methyl glycosides with GC-MS (electron impact) analysis (York et al. 1985; Forsberg et al. 2003) using a 30-m DB-5 capillary column (J&W Scientific). The SCWP preparations were free of amino acids as determined by analysis of the heptafluorobutyrate derivatives (Zanetta et al. 1999), with GC-MS analysis using a HP-5 capillary column. The absolute configuration of glycosyl residues was determined by preparing the diastereomeric TMS (±)-2-butyl glycoside derivatives (Gerwig et al. 1979), with GC-MS analysis on a DB-1 column with comparisons to authentic D-Gal, D-GlcNAc and D-ManNAc derivatives. Glycosyl linkage analysis was performed according to a modification of the method of Ciucanu and Kerek (1984) as described previously (Choudhury et al. 2006). The resulting partially methylated alditol acetates were dissolved in dichloromethane and analyzed by GC-MS using a DB-1 or SP-2330 capillary column as described (Choudhury et al. 2006; Forsberg and Carlson 2008).

Mass spectrometry

Samples of the SCWP and derived oligosaccharides were analyzed by MALDI-TOF mass spectrometry, using an Applied Biosystems 4700 instrument. The sample was dissolved in water at 10 µg/µL and mixed in equal proportion (v/v) with 0.5 M Super-DHB (2,5-dihydroxy/2-hydroxy-5-methoxy benzoic acid; Sigma-Aldrich) as matrix. Spectra were acquired in positive ion and reflectron mode with acceleration voltage of 20 kV. The predicted MM of the various saccharides was calculated using the following average incremental mass values, based on the atomic weights of the elements: hexose, 162.142; 2-*N*-acetamido-2-deoxyhexose, 203.195; free reducing end, 18.0153.

Nuclear magnetic resonance analyses

^{1}H spectra and all two-dimensional homo- and heteronuclear spectra of the SCWPs were recorded at 25°C on a Varian Inova 600 MHz or Varian 800 MHz spectrometer, each equipped with a 3-mm cryogenic probe, using Varian software (Varian Medical Systems, Palo Alto, CA). The SCWPs released by HF treatment, and purified by Superose-12 chromatography, were dissolved in 200 µL of D_2O yielding clear solutions at ∼7 mg/mL in 3 mm tubes; spectra were referenced to internal 2,2-dimethyl-2-silapentane-5-sulfonate sodium salt (DSS) at δ_H 0.00 ppm.

^{1}H-^{1}H COSY (Piantini et al. 1982) data were recorded in the absolute value mode with a 6.10 ppm spectral width and a matrix size of 1024 × 4096 complex points with eight scans per increment. ^{1}H-^{1}H zTOCSY (Bax and Davis 1985) was recorded with a mixing time of 150 ms and a matrix of 400 × 4096 at 32 scans per increment. Nuclear Overhauser effect analysis (Macura et al. 1981) was performed by phase-sensitive ^{1}H-^{1}H NOESY experiments, collected with a 150 ms mixing time and matrix size identical to that used for zTOCSY, with 64 scans per increment. Carbon chemical shifts and carbon-proton one-bond correlations were determined with a gradient-selected ^{1}H-^{13}C HSQC (Davis et al. 1991) collected in the ^{1}H-detection mode. The acquisition time was 0.2 s, and the matrix size was typically 256 × 2000 complex points, at 88–144 scans per increment with multiplicity distinction for primary or secondary protons. The coupling constant ($^{1}J_{CH}$) was set to 150 Hz and the carbon spectral width was 110 ppm, with transmitter offset of 65 ppm. Phase-sensitive ^{1}H-^{13}C HMBC spectra were acquired with 256 × 2048 complex points at 96–144 scans per increment. The carbon and proton sweep widths were identical to HSQC values, and the acquisition time (t2) was 0.27 s. The HMBC transfer delay was set to 50 ms (10 Hz), and 1-bond J-filter was 150 Hz. Anomeric configurations of the glycosyl linkages were assigned from carbon-proton coupling constants ($J_{C1,H1}$) measured for the native SCWP by ^{1}H-^{13}C HSQC analysis without ^{13}C decoupling. The acquisition time was 0.6 s, collecting 128 scans per increment; the coupling constant ($^{1}J_{CH}$) was set to 160 Hz and carbon sweep width was 80–120 ppm. ^{1}H-^{13}C HSQC-TOCSY spectra were recorded for the SCWP on the 600 MHz instrument, with a matrix size of 512 × 2048 collecting 32 scans per increment and mixing time of 30 ms.

Supplementary data

Supplementary data for this article is available online at http://glycob.oxfordjournals.org/.

Funding

This work was supported in part by National Institutes of Health (R21 AI076753 to R.W.C.). The Complex

Carbohydrate Research Center was supported in part by Department of Energy (DE-FG02-93ER20097).

Acknowledgements

The authors are grateful to John Glushka for assistance with NMR analyses. The findings and conclusions in this report are those of the author(s) and do not necessarily represent the views of the Centers for Disease Control and Prevention. Patent Pending—University of Georgia Research Foundation, Inc. and US Centers for Disease Control and Prevention.

Abbreviations

COSY, ^{1}H-^{1}H correlation spectroscopy; DSS, 2,2-dimethyl-2-silapentane-5-sulfonate, sodium salt; Gal, galactose; GC-MS, gas–liquid chromatography-mass spectrometry; GlcNAc, *N*-acetylglucosamine; HF, hydrofluoric acid; HMBC, heteronuclear multiple bond coherence spectroscopy; HSQC, heteronuclear single quantum coherence spectroscopy; MALDI-TOF, matrix-assisted laser desorption ionization-time of flight; ManNAc, *N*-acetylmannosamine; MLST, multilocus sequence typing; MM, molecular mass; NMR, nuclear magnetic resonance; NOESY, nuclear Overhauser effect spectroscopy; SEC, size exclusion chromatography; SCWP, secondary cell wall polysaccharide; TMS, trimethylsilyl; TOCSY, total correlation spectroscopy.

References

Bax A, Davis DG. 1985. MLEV-17-based two-dimensional homonuclear magnetization transfer spectroscopy. *J Magn Reson*. 65:355–360.

Brown WC. 1973. Rapid methods for extracting autolysins from *Bacillus subtilis*. *Appl Microbiol*. 25:295–300.

CDC. 1990. Foodborne disease outbreaks, 5-year summary, 1983–1987. Morbidity and Mortality Weekly Report. Atlanta (GA): CDC.

CDC. 1996. Surveillance for foodborne-disease outbreaks United States 1888–1992. Morbidity and Mortality Weekly Report. Atlanta (GA): CDC.

Choudhury B, Leoff C, Saile E, Wilkins P, Quinn CP, Kannenberg EL, Carlson RW. 2006. The structure of the major cell wall polysaccharide of *Bacillus anthracis* is species-specific. *J Biol Chem*. 281:27932–27941.

Ciucanu I, Kerek F. 1984. A simple and rapid method for the permethylation of carbohydrates. *Carbohydr Res*. 131:209–217.

Davis AL, Laue ED, Keeler J, Moskau D, Lohman J. 1991. Absorption mode two-dimensional NMR spectra recorded using pulse field gradients. *J Magn Reson*. 94:637–644.

Forsberg LS, Carlson RW. 2008. Structural characterization of the primary *O*-antigenic polysaccharide of the *Rhizobium leguminosarum* 3841 lipopolysaccharide and identification of a new 3-acetimidoylamino-3-deoxyhexuronic acid glycosyl component. *J Biol Chem*. 283:16037–16050.

Forsberg LS, Noel KD, Box J, Carlson RW. 2003. Genetic locus and structural characterization of the biochemical defect in the *O*-antigenic polysaccharide of the symbiotically deficient *Rhizobium etli* mutant, CE166: Replacement of *N*-acetylquinovosamine with its hexosyl-4-ulose precursor. *J Biol Chem*. 278:51347–51359.

Gerwig GJ, Kamerling JP, Vliegenthart JFG. 1979. Determination of the absolute configuration of monosaccharides in complex carbohydrates by capillary GLC. *Carbohydr Res*. 77:1–7.

Hoffmaster A, Novak R, Marston C, Gee J, Helsel L, Pruckler J, Wilkins P. 2008. Genetic diversity of clinical isolates of *Bacillus cereus* using multilocus sequence typing. *BMC Microbiol*. 8:191.

Hoffmaster AR, Hill KK, Gee JE, Marston CK, De BK, Popovic T, Sue D, Wilkins PP, Avashia SB, Drumgoole R, et al. 2006. Characterization of *Bacillus cereus* isolates associated with fatal pneumonias: Strains are closely related to *Bacillus anthracis* and harbor *B. anthracis* virulence genes. *J Clin Microbiol*. 44:3352–3360.

Hoffmaster AR, Ravel J, Rasko DA, Chapman GD, Chute MD, Marston CK, De BK, Sacchi CT, Fitzgerald C, Mayer LW, et al. 2004. Identification of anthrax toxin genes in a *Bacillus cereus* associated with an illness resembling inhalation anthrax. *Proc Natl Acad Sci*. 101:8449–8454.

Kern J, Ryan C, Faull K, Schneewind O. 2010. *Bacillus anthracis* surface-layer proteins assemble by binding to the secondary cell wall polysaccharide in a manner that requires csaB and tagO. *J Mol Biol*. 401:757–775.

Kiel JA, Boels JM, Beldman G, Venema G. 1994. Glycogen in *Bacillus subtilis*: Molecular characterization of an operon encoding enzymes involved in glycogen biosynthesis and degradation. *Mol Microbiol*. 11:203–218.

Klee SR, Brzuszkiewicz EB, Nattermann H, Brüggemann H, Dupke S, Wollherr A, Franz T, Pauli G, Appel B, Liebl W, et al. 2010. The genome of a *Bacillus* isolate causing anthrax in chimpanzees combines chromosomal properties of *B. cereus* with *B. anthracis* virulence plasmids. *PLoS ONE*. 5:e10986.

Klee SR, Ozel M, Appel B, Boesch C, Ellerbrok H, Jacob D, Holland G, Leendertz FH, Pauli G, Grunow R, et al. 2006. Characterization of *Bacillus anthracis*-like bacteria isolated from wild great apes from Cote d'Ivoire and Cameroon. *J Bacteriol*. 188:5333–5344.

Leoff C, Choudhury B, Saile E, Quinn CP, Carlson RW, Kannenberg EL. 2008. Structural elucidation of the nonclassical secondary cell wall polysaccharide from *Bacillus cereus* ATCC 10987. *J Biol Chem*. 283:29812–29821.

Leoff C, Saile E, Rauvolfova J, Quinn CP, Hoffmaster AR, Zhong W, Mehta AS, Boons GJ, Carlson RW, Kannenberg EL. 2009. Secondary cell wall polysaccharides of *Bacillus anthracis* are antigens that contain specific epitopes which cross-react with three pathogenic *Bacillus cereus* strains that caused severe disease, and other epitopes common to all the *Bacillus cereus* strains tested. *Glycobiology*. 19:665–673.

Leoff C, Saile E, Sue D, Wilkins P, Quinn CP, Carlson RW, Kannenberg EL. 2008. Cell wall carbohydrate compositions of strains from the *Bacillus cereus* group of species correlate with phylogenetic relatedness. *J Bacteriol*. 190:112–121.

Lipkind GM, Shashkov AS, Knirel YA, Vinogradov EV, Kochetkov NK. 1988. A computer-assisted structural analysis of regular polysaccharides on the basis of ^{13}C-NMR data. *Carbohydr Res*. 175:59–75.

Macura S, Huang Y, Suter D, Ernst RR. 1981. Two-dimensional chemical exchange and cross-relaxation spectroscopy of coupled nuclear spins. *J Magn Reson*. 43:259–281.

Mesnage S, Fontaine T, Mignot T, Delepierre M, Mock M, Fouet A. 2000. Bacterial SLH domain proteins are non-covalently anchored to the cell surface via a conserved mechanism involving wall polysaccharide pyruvylation. *EMBO J*. 19:4473–4484.

Mesnage S, Tosi-Couture E, Mock M, Fouet A. 1999. The S-layer homology domain as a means for anchoring heterologous proteins on the cell surface of *Bacillus anthracis*. *J Appl Microbiol*. 87:256–260.

Miller JM, Hair JG, Hebert M, Hebert L, Roberts FJ, Jr., Weyant RS. 1997. Fulminating bacteremia and pneumonia due to *Bacillus cereus* [published erratum appears in J Clin Microbiol 1997 May;35(5):1294]. *J Clin Microbiol*. 35:504–507.

Piantini U, Sörensen OW, Ernst RR. 1982. Multiple quantum filters for elucidating NMR coupling networks. *J Am Chem Soc*. 104:6800–6801.

Schäffer C, Messner P. 2005. The structure of secondary cell wall polymers: How Gram-positive bacteria stick their cell walls together. *Microbiology*. 151:643–651.

Slock JA, Stahly DP. 1974. Polysaccharide that may serve as a carbon and energy storage compound for sporulation in *Bacillus cereus*. *J Bacteriol*. 120:399–406.

Takata H, Takaha T, Okada S, Takagi M, Imanaka T. 1997. Characterization of a gene cluster for glycogen biosynthesis and a heterotetrameric ADP-glucose pyrophosphorylase from *Bacillus stearothermophilus*. *J Bacteriol*. 179:4689–4698.

York WS, Darvill AG, McNeil M, Stevenson TT, Albersheim P. 1985. Isolation and characterization of plant cell walls and cell wall components. *Meth Enzymol*. 118:3–40.

Zanetta JP, Timmerman P, Leroy Y. 1999. Gas–liquid chromatography of the heptafluorobutyrate derivatives of the *O*-methyl-glycosides on capillary columns: A method for the quantitative determination of the monosaccharide composition of glycoproteins and glycolipids. *Glycobiology*. 9:255–266.